Geochimica et Cosmochimica Acta, Vol. 68, No. 24, pp. 5127–5138, 2004

0016-7037/04 $30.00 + .00

doi:10.1016/j.gca.2004.06.002

Argon and CO_2 on the race track in silicate melts: A tool for the development of a CO_2 speciation and diffusion model

Marcus Nowak,* Dominik Schreen, and Kai Spickenbom
Institut für Mineralogie, Universität Hannover, Callinstrasse 3, 30167 Hannover, Germany

(*Received February* 16, 2004; *accepted in revised form June* 7, 2004)

Abstract—We have analysed the kinetics of Argon and CO_2 diffusion in simplified iron free rhyolitic to hawaiitic melts using the diffusion couple technique. The concentration distance profiles of Ar and CO_2 were measured with electron microprobe analysis and Fourier Transform Infrared Spectroscopy, respectively. Error functions were fitted to the symmetrical concentration distance profiles to extract the diffusion coefficients.

In the temperature range 1373 to 1773 K the activation energies for Ar diffusion range from 169 ± 20 to 257 ± 62 kJ mol^{-1}. Ar diffusivity increases exponentially with the degree of depolymerisation. In contrast, the mobility of total CO_2, that is identical to Ar mobility in rhyolitic melt, keeps constant with changing bulk composition from rhyolite to hawaiite. CO_2 speciation at 1623 K and 500 MPa was modeled for the range of compositions studied using the diffusion data of Ar and total CO_2 in combination with network former diffusion calculated from viscosity data. Within error this model is in excellent agreement with CO_2 speciation data extrapolated from temperatures near the glass transition temperature for dacitic melt composition. This model shows that even in highly depolymerised hawaiitic and tholeiitic melts molecular CO_2 is a stable species and contributes 70 to 80% to the total CO_2 diffusion, respectively.

1. INTRODUCTION

Argon is the most abundant noble gas dissolved in terrestrial magmas and in the atmosphere. Argon solubility and mobility in silicate melts play a fundamental role in understanding the degassing history of the Earth driven by magmatic transport from the mantle to the surface and subsequent degassing. The main focus of laboratory studies has been the investigation of Ar diffusion in fully polymerised silicate melts (Carroll, 1991; Carroll and Stolper, 1991; Roselieb et al., 1992, 1995; Behrens and Zhang, 2001). A knowledge of transport properties of Ar in depolymerised melts is necessary for understanding the transport of complex volatile species, such as CO_2, which may also diffuse as neutral molecules (Sierralta et al., 2002). Next to H_2O, CO_2 is the second most abundant volatile dissolved in magmas. CO_2 plays an important role in the degassing processes of ascending magmas and volcanic areas (Holloway, 1976; Papale and Polacci, 1999). Even small amounts of dissolved CO_2 shift the fluid saturation limit of hydrous magmas to greater depth implying that CO_2 is an important driving force for bubble formation in ascending magmas. For this reason, knowledge on the mobility and diffusion mechanisms of CO_2 in silicate liquids is of fundamental importance for understanding bubble growth and dynamic degassing processes that control volcanic eruption styles.

Spectroscopic measurements of CO_2-bearing aluminosilicate glasses have shown that CO_2 is present as molecular CO_2 and CO_3^{2-} groups linked to the silicate network (Mysen and Virgo, 1980; Fine and Stolper, 1985; Kohn et al., 1991; Brooker et al., 1999, 2001a; Sierralta et al., 2002; Nowak et al., 2003), although more independent and mobile 'ionic carbonate pairs' may also exist in highly peralkaline compositions (Brooker, 2001b). The ratio of the CO_2 species concentrations depends strongly on bulk composition of the glass. In fully polymerised rhyolitic glasses, CO_2 is incorporated as molecular CO_2 and in depolymerised basaltic glasses, CO_2 is present as CO_3^{2-}. In albitic, dacitic, and jadeitic glasses/melts near the glass transition temperature, CO_2 is incorporated as both molecular CO_2 and CO_3^{2-} fixed to the network structure. It has recently been shown that in these melts the equilibrium of the homogeneous species reaction CO_2 (melt) + O^{2-} (melt) = CO_3^{2-} (melt) shifts towards molecular CO_2 with increasing temperature (Morizet et al., 2001; Porbatzki and Nowak, 2001; Nowak et al., 2003). This implies that even in depolymerised silicate melts, (1) a significant proportion of total CO_2 is dissolved as molecular CO_2 and consequently, (2) the mobility of molecular CO_2 might contribute significantly to the diffusivity of bulk CO_2.

Behrens and Zhang (2001) have recently shown that in rhyolitic melt Ar diffusion is comparable to molecular CO_2 diffusion. Therefore, we used Ar as a monitor for molecular CO_2 diffusion to shed light on total CO_2 diffusion mechanisms. For this purpose we performed diffusion couple experiments at 500 MPa of the inert component Ar at 1373 to 1773 K and of the reactive component CO_2 at 1623 K in simplified natural melts from iron free highly polymerised rhyolitic to strongly depolymerised hawaiitic melts in an internally heated argon pressure vessel.

2. EXPERIMENTAL AND ANALYTICAL METHODS

2.1. Glass Synthesis

Batches of 5 to 10 g melt with simplified iron free rhyolitic (Rh), dacitic (Da), dacitic-andesitic (DaAn), andesitic (An), andesitic-tholeiitic (AnTh), tholeiitic (Th), and hawaiitic (Ha) compositions based on compositions given by Philpotts (1990) were synthesized in Pt crucibles by fusion of dried, mixed, and homogenised powders of SiO_2, TiO_2, Al_2O_3, MgO, $CaCO_3$, Na_2CO_3, and K_2CO_3 in a high temperature furnace at 1873 K. Iron oxide was substituted by equal molar amounts

* Author to whom correspondence should be addressed (m.nowak@mineralogie.uni-hannover.de).

of MgO. After melting the crucibles were quenched rapidly in cold water to form glasses. Rapid cooling caused several tension cracks within the glass, forming pieces of ~0.5 to 1 cm^3 that could easily be removed from the crucibles. Glass pieces from each batch were prepared for electron microprobe analysis (Cameca SX 100) to measure the glass compositions and to test for homogeneity. Microprobe analytical conditions were 15 kV acceleration voltage, 6 nA beam current and 2 to 5 s counting time for each element. The beam was defocused to 20 μm to optimise the analysis of Na. Glass compositions are given in Table 1. The glasses were crushed in a steel mortar and sieved to grain sizes of <200 μm for the synthesis of volatile free and volatile bearing glass cylinders.

2.2. Synthesis of Glass Cylinders for Diffusion Couple Experiments

To synthesize glass cylinders for argon diffusion, platinum capsules (6.4 mm in diameter, 35 mm in length, and 0.2 mm in wall thickness) were welded shut at the bottom and glass powders were packed into the capsules using a tightly fitting hard metal rod to compress the powders. For the synthesis of Ar-free glass cylinders the filled capsules (3 mm in diameter, 35 mm in length, 0.2 mm in wall thickness) were dried at 383 K for one hour and subsequently welded shut. Filled capsules for the synthesis of argon bearing depolymerised An to Ha glasses were carefully crimped, ensuring that a thin slit remained for a pathway of the pressure medium Ar into the capsule. Capsules for synthesis of highly polymerized Ar-bearing Rh, Da and DaAn glass cylinders (6.4 mm in diameter, 35 mm in length, 0.2 mm in wall thickness) were carefully crimped together with a 0.3 mm Pt wire. After crimping the wire was removed so that the remaining small hole ensured a pathway for Ar gas. The glass samples were melted at 1623 K and 400–450 MPa for 1h (Ar-free) to 72 h (Ar-bearing) in an internally heated argon pressure vessel (IHPV). After the runs the samples were isobarically quenched to room temperature by turning off the power of the furnace. The initial cooling rate of the samples was measured to be ~3.3 K s^{-1}. This cooling was rapid enough to avoid quench crystal formation in the depolymerised melts. Initial synthesis of the highly polymerized Ar-bearing samples (Rh-DaAn) produced bubble-rich glasses. These foamy glasses were crushed again to glass powder, filled in 3 mm Pt capsules, compressed, welded shut and re-melted at 500 MPa and 1623 K for 1 h. The resulting glass cylinders were free of bubbles or contained only few small bubbles <5 μm probably filled with Ar indicating gas saturation.

Glass cylinders with and without CO_2 for diffusion experiments were synthesized in Au80Pd20 capsules (3 mm in diameter, 30 mm in length, 0.2 mm in wall thickness). Sierralta et al. (2002) have recently demonstrated that in contrast to Pt capsule material, CO_2-bearing glass cylinders synthesized in Au80Pd20 capsules show no CO_2 loss and zoning of CO_2 concentration towards the capsule walls. Silver oxalate ($Ag_2C_2O_4$) equivalent to 0.2 wt% CO_2 was used as the CO_2 source. Details for capsule preparation are given in Sierralta et al. (2002) and Nowak et al. (2003). The syntheses were run at 1623 K and 500 MPa in the IHPV at intrinsic oxidising conditions equivalent to the MnO-Mn_3O_4 solid oxygen buffer ($\log f O_2$ = QFM + 4) (Berndt et al., 2002).

The bubble-free and transparent glasses were not removed from the noble metal as this helps to maintain the glass integrity whilst 4 to 5 mm long cylinders were sawn from the capsules. The exposed glass surfaces were polished with 3 μm diamond paste. In addition 1 mm thick slabs were sawn from the middle of the cylinders and were prepared for electron microprobe and infrared analysis.

2.3. Diffusion Couple Experiments

The diffusion couple technique using a cylindrical geometry described by Nowak and Behrens (1997) and Sierralta et al. (2002) was used to obtain one-dimensional semi-infinite medium diffusion profiles of Ar and total CO_2. Noble metal jacketed volatile bearing glass cylinders were brought into contact with volatile free glass cylinders of the same glass composition and welded shut in 4 mm Pt capsules for Ar diffusion and in 4 mm Au80Pd20 capsules for CO_2 diffusion. The experiments were performed using an IHPV with a heating rate of 0.5 K s^{-1} and an initial cooling rate of 3.3 K s^{-1}. Run pressure was 500 MPa for all diffusion experiments. Run temperatures for the Ar diffu-

Table 1. Bulk compositions based on 10 measurements and volatile contents of glasses (in wt%) for diffusion experiments. 1σ errors are given in parentheses.

	SiO_2	TiO_2	Al_2O_3	MgO	CaO	Na_2O	K_2O	Total	*NBO/T* (dry)	*IP*[a] %	H_2O	CO_2,total[b]	Ar
Rh (Ar)	74.39 (79)	0.23 (4)	14.08 (50)	1.56 (12)	1.36 (13)	3.80 (22)	4.11 (15)	99.53 (21)	0.039	49.49	0.27 (4)	—	0.271 (5)[c]
Rh (CO_2)	75.09 (80)	0.22 (2)	13.83 (27)	1.47 (5)	1.40 (3)	3.86 (11)	4.10 (5)	99.99 (62)	0.041		0.07 (2)	0.22 (2)	—
Da (Ar)	71.26 (60)	0.44 (5)	15.21 (23)	2.40 (11)	2.79 (15)	4.60 (26)	2.99 (13)	99.69 (54)	0.089	49.28	n. d.	—	0.235 (2)[c]
Da (CO_2)	71.78 (86)	0.40 (3)	15.31 (21)	2.26 (6)	3.09 (11)	4.52 (10)	2.97 (4)	100.33 (69)	0.087		0.05 (2)	0.20 (2)	—
DaAn (Ar)	66.76 (40)	0.81 (6)	15.88 (20)	5.38 (15)	4.50 (14)	4.21 (19)	1.94 (10)	99.48 (62)	0.204	48.82	0.09 (2)	—	0.169 (2)[c]
DaAn (CO_2)	66.13 (47)	0.68 (5)	16.18 (34)	4.59 (11)	4.79 (10)	4.26 (18)	1.90 (11)	98.53 (56)	0.182		0.07 (2)	0.20 (2)	—
An (Ar)	61.89 (43)	1.18 (4)	16.83 (24)	8.48 (17)	6.39 (15)	4.11 (32)	0.92 (5)	99.80 (52)	0.342	48.30	0.07 (2)	—	0.166 (3)[d]
An (CO_2)	63.37 (39)	1.11 (4)	16.90 (20)	8.08 (10)	6.81 (8)	4.04 (11)	0.88 (2)	101.25 (29)	0.33		0.06 (2)	0.19 (2)	—
AnTh (Ar)	60.49 (37)	1.75 (10)	15.53 (24)	9.83 (22)	7.35 (19)	3.57 (23)	1.20 (9)	99.71 (61)	0.439	48.08	n. d.	—	0.168 (2)[d]
AnTh (CO_2)	61.92 (32)	1.55 (4)	15.22 (14)	8.79 (12)	6.74 (13)	3.73 (16)	1.33 (7)	99.57 (41)	0.391		0.08 (2)	0.20 (2)	—
Th (Ar)	57.99 (50)	2.37 (12)	14.80 (30)	11.08 (29)	8.64 (32)	3.13 (22)	1.58 (7)	99.57 (52)	0.546	47.81	0.10 (2)	—	0.071 (2)[d]
Th (CO_2)	60.48 (27)	2.01 (2)	14.54 (19)	9.95 (10)	8.79 (11)	3.32 (9)	1.61 (6)	100.55 (24)	0.504		0.07 (2)	0.19 (2)	—
Ha (Ar)	51.73 (22)	4.06 (14)	17.25 (24)	11.81 (19)	8.76 (21)	4.56 (29)	1.59 (12)	99.76 (54)	0.593	47.40	n. d.	—	0.051 (2)[d]
Ha (CO_2)	53.55 (34)	3.74 (4)	16.93 (17)	11.32 (8)	9.19 (12)	4.71 (7)	1.44 (4)	100.88 (26)	0.583		0.06 (2)	0.20 (2)	—

[a] *IP* = ionic porosity in %.
[b] CO_2 concentrations determined by weight considering the measured CO_2 yield of silver oxalate that is 95.9 % of the expected value.
[c] Run conditions = 1623 K, 450 MPa.
[d] Run conditions = 1623 K, 400 MPa.

Table 2. Run conditions of diffusion experiments and diffusion coefficients of Ar and CO_2.

Run no.	T (K)	t_{nom} (s)[a]	t_{eff} (s)[b]	log$D$ (D in m^2 s^{-1})
Rh01-Ar[c]	1373	40320	40327 (60)	−12.22 (10)
Rh02-Ar	1473	15780	15804 (60)	−11.71 (10)
Rh03-Ar	1573	7020	7106 (60)	−11.18 (10)
Rh04-Ar	1623	4800	4909 (60)	−11.05 (10)
Rh04-Ar	1673	3420	3639 (60)	−10.92 (10)
Rh05-Ar	1673	2460	2644 (60)	−10.85 (10)
Rh06-Ar	1723	2460	2737 (60)	−10.76 (10)
Rh07-Ar	1773	1800	2233 (60)	−10.74 (10)
Da01-Ar[c]	1473	15780	15816 (60)	−11.74 (10)
Da02-Ar	1523	10380	10436 (60)	−11.43 (10)
Da03-Ar	1573	7020	7116 (60)	−11.20 (10)
Da05-Ar	1623	4800	4917 (60)	−11.10 (10)
Da04-Ar	1673	3420	3642 (60)	−10.91 (10)
Da06-Ar	1723	2460	2751 (60)	−10.86 (10)
Da07-Ar	1773	1800	2233 (60)	−10.64 (10)
DaAn01-Ar	1573	7020	7086 (60)	−11.26 (10)
DaAn02-Ar	1623	4800	4897 (60)	−10.99 (10)
DaAn03-Ar	1673	3420	3580 (60)	−10.83 (10)
DaAn04-Ar	1723	2460	2709 (60)	−10.69 (10)
DaAn05-Ar	1773	1800	2077 (60)	−10.63 (10)
An01-Ar	1623	4800	4879 (60)	−11.01 (10)
An02-Ar	1673	3420	3560 (60)	−10.71 (10)
An03-Ar	1723	2460	2663 (60)	−10.61 (10)
An04-Ar	1773	1800	2123 (60)	−10.52 (10)
AnTh01-Ar	1623	4800	4863 (60)	−10.95 (10)
AnTh02-Ar	1673	3420	3534 (60)	−10.72 (10)
AnTh03-Ar	1723	2460	2643 (60)	−10.55 (10)
AnTh04-Ar	1773	1800	2114 (60)	−10.39 (10)
Th01-Ar	1623	4800	4941 (60)	−10.68 (10)
Th02-Ar	1673	3420	3630 (60)	−10.38 (10)
Th03-Ar	1723	2460	2752 (60)	−10.27 (10)
Th04-Ar	1773	1800	2026 (60)	−9.95 (10)
Ha01-Ar	1623	4800	4842 (60)	−10.55 (10)
Ha02-Ar	1673	3420	3507 (60)	−10.51 (10)
Ha03-Ar	1723	2460	2610 (60)	−10.05 (10)
Ha04-Ar	1773	1800	2084 (60)	−9.92 (10)[d]
Rh01-CO2	1623	3600	3798 (60)	−11.10 (15)
Da01-CO2	1623	3600	3798 (60)	−11.35 (15)
DaAn01-CO2	1623	3600	3798 (60)	−11.14 (15)
DaAn02-CO2	1623	14520	14718 (60)	−11.18 (15)
An01-CO2	1623	14400	14598 (60)	−11.23 (15)
AnTh03-CO2	1623	15060	15258 (60)	−11.09 (15)
Th01-CO2	1623	3600	3798 (60)	−11.14 (15)
Ha01-CO2	1623	3600	3798 (60)	−11.18 (15)

[a] t_{nom} = nominal run time from reaching run temperature to starting of cooling the experiment.

[b] t_{eff} = effective run time considering heating and cooling calculated as outlined by Nowak and Behrens (1997).

[c] Samples contain few small crystals.

[d] The logD_{Ar} of −9.92 is the average of 7 Ar diffusion coefficients determined from concentration distance profiles measured with an offset of n × 350 μm (n = 1 − 7) perpendicular to the diffusion direction of Ar. The standard deviation of the mean is ±0.05 log unit.

sion experiments were 1373 to 1773 K. Carbon dioxide diffusion experiments were performed at 1623 K. Run times were 0.5 to 11.2 h. Experimental details are given in Table 2. The melts were not affected by degassing and bubble formation because at the chosen P and T conditions the melts were volatile undersaturated. Furthermore the run times were short enough to preserve the initial volatile contents at both ends of the diffusion couples allowing the application of a simple one-dimensional diffusion equation for semi-infinite medium configuration. After the runs, 300 to 400 μm thick slabs were sawn out of the capsules along the cylinder axis and thus parallel to the diffusion direction of the volatiles. Ar-bearing slabs were ground and polished to thicknesses of 30 μm and fixed on glass slides for microprobe analysis. Furthermore, Ar-bearing slabs were ground and polished on both sides to a thickness of 260 μm and fixed on glass slides with slits 2 mm wide and 20 mm long for infrared analysis of H_2O content. CO_2-bearing slabs for infrared analysis were ground and polished on both sides to a thickness of ~100 μm. The slabs were also fixed on glass slides as described above for infrared analysis.

2.4. Determination of Concentration Distance Profiles Using Microprobe Analysis for Ar and Infrared Spectroscopy for CO_2

The electron microprobe CAMECA SX 100 was used to measure Ar concentration distance profiles along traverses perpendicular to the original interface of the diffusion sample following the diffusion direction of Ar. A SiO_2 glass containing 1.01 wt% Ar (K. Roselieb, private communication) was used for calibration. Microprobe analytical conditions were 15 kV acceleration voltage, 140 nA beam current, focussed beam, and 30 s counting time for Ar following the analytical conditions of Roselieb et al. (1996) and Behrens and Zhang (2001). At the chosen analytical conditions the detection limit of Ar concentration is ~0.006 wt%. Analyses were performed in 8 to 100 μm steps adjusted by a digitally controlled X-Y table parallel to the diffusion direction of Ar.

A Bruker IFS 88 with an IR-scope II microscope, using a globar light source, a KBr beamsplitter, an InSb-MCT sandwich detector, and a resolution of 2 cm^{-1} was used for measuring mid-infrared (MIR) spectra. The spectrometer and the microscope were flushed with dried air, to minimize interferences due to changes in the H_2O contents of the air. Reference spectra were taken after every tenth measurement to minimize possible interferences with atmospheric CO_2. Spectra were collected with 32 scans per analysed area. An aperture of 100 × 100 μm was used to measure MIR spectra for the determination of H_2O and CO_2 concentrations in the samples synthesized for diffusion experiments. For measuring CO_2 concentration distance profiles, a slit aperture of 15 × 200 μm width was adjusted to maintain a spatial resolution of 30 μm parallel to the diffusion profile of CO_2. Spectra were collected in 10 to 100 μm steps adjusted by a digitally controlled X-Y table parallel to the diffusion direction of CO_2.

3. RESULTS

3.1. Solubility Data of Ar in Silicate Melts

Argon concentrations in the glass cylinders synthesized for diffusion experiments were determined with electron microprobe. 10 measurements were performed horizontally and vertically on each glass slide. The Ar solubilities are summarized in Table 1. At 1623 K and 450 MPa Ar solubility decreases from 0.271 ± 0.005 wt % in Rh melt to 0.169 ± 0.002 wt% in DaAn melt. At 1623 K and 400 MPa Ar solubility decreases from 0.166 ± 0.003 wt% in An melt to 0.051 ± 0.002 wt% in Ha melt. Our Ar solubility results are in good agreement with Ar solubility data of Carroll and Stolper (1993) in silicate melts. The ionic porosity model for Ar solubility in silicate melts (Carroll and Stolper, 1993) based on the density model of silicate melts (Lange and Carmichael, 1987) and on the corresponding volume of cations and anions (ionic radii given by Shannon and Prewitt, 1969) was used to compare the dissolved Ar contents at different pressures (400–450 MPa). Carroll and Stolper (1993) have parameterised the effects of temperature, pressure, and melt composition on Ar solubility. Ionic porosity is defined as:

$$IP = 100 \cdot \left(1 - \frac{V_{ca}}{V_m}\right) \quad (1)$$

where IP is the ionic porosity in %, V_{ca} is the total volume of cations and anions in 1 g of melt and V_m is the specific melt

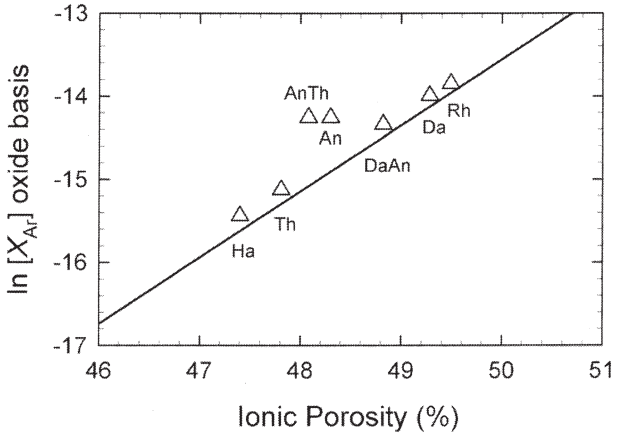

Fig. 1. Solubility of Ar expressed as natural logarithm of mole fraction based on 1 mol of oxide components dissolved at one bar gas pressure vs. ionic porosity in %. Errors in ln[X_{Ar}] are about the symbol size. The solid line represents Ar solubility based on the model of Carroll and Stolper (1993). For details see text.

volume (cm^3/g) (Dowty, 1980; Fortier and Giletti, 1989). In Figure 1 measured Ar concentrations are expressed as mole fractions of dissolved gas normalized to 1 bar and based on 1 mol of oxide components of the melt compositions. The measured Ar solubility increases significantly with ionic porosity. Although our synthesis experiments were not designed for solubility experiments, the measured Ar concentrations match the linear least square regression for Ar solubility of Carroll and Stolper (1993) within 0.5 natural log units. In contrast to claims of Shibata et al. (1998) the Argon solubilities do not follow a *NBO/T* (degree of depolymerisation expressed as non-bridging oxygens per tetrahedron) relationship (especially An and AnTh) any better than the *IP* correlation.

3.2. Total CO_2 and Ar Concentration Distance Profiles

Spectra of volatile-free background corrected CO_2-bearing Rh to Ha glasses normalized to 100 μm thickness are shown in Figure 2. Spectra of the CO_2-free parts of the diffusion samples were measured for reference. Subtraction of the spectrum of the CO_2-free part from the spectrum of the CO_2-bearing part of the diffusion samples result in separation of the ν_3 asymmetric stretch band of distorted CO_3^{2-} at 1750 to 1300 cm^{-1} from the lattice overtone vibrations at 1750 to 1550 cm^{-1} and the high frequency flank of the fundamental Si-O stretching mode. The sharp absorption band at 2350 cm^{-1} is due to the ν_3 asymmetric stretch vibration of dissolved molecular CO_2 (Brey and Green, 1975; Nakamoto et al., 1957; White, 1974). In addition, the Rh and Da spectra show small absorption features near the detection limit located between 2100 and 2200 cm^{-1}. There might be two explanations for these small band features: (1) These absorption features might be artefacts of the volatile free background subtraction procedure. The CO_2-free and the CO_2-bearing part of the diffusion samples contain slightly different amounts of H_2O (~0.04 wt%). We suggest that these differences might slightly affect the high frequency flank of overtones of fundamental Si-O vibrations that are pronounced in SiO_2-rich glass compositions as suggested by Fogel and Rutherford (1990) and Blank and Brooker (1994). (2) The absorption band might be due to molecular CO that is located at ~2160 cm^{-1} (Pawley et al., 1992). Kohn et al. (1991), Blank and Brooker (1994), and Brooker et al. (1999) identified molecular CO in reduced graphite-bearing albitic and rhyolitic glasses containing graphite using ^{13}C MAS NMR spectroscopy and infrared spectroscopy. Some molecular CO solubility might be expected at reducing conditions as this molecule is smaller than molecular CO_2 and thus should fit into available sites in the silicate melt structure. In contrast, our CO_2-bearing samples were synthesized at oxidising conditions (QFM + 4). As a result the samples were clear and colourless indicating absence of graphite. Thus it seems to be unlikely that in our synthesis experiments molecular CO is a stable species that might contribute to total CO_2 diffusion.

The peak areas of molecular CO_2 and CO_3^{2-} were determined from the background subtracted spectra. We have assumed that the CO_2 species ratio is independent of bulk CO_2 in the concentration range 0 to 0.2 wt% (e. g. Stolper et al., 1987). Assuming absorbance coefficients remain constant, the absorbance peaks for either species can be considered as directly proportional to the bulk CO_2 concentration and as a result either species can be used as an indicator of the relative CO_2 concentration change.

Representative Ar and total CO_2 concentration distance profiles are presented in Figure 3. Argon and total CO_2 diffusion coefficients were obtained from least-square fits of a modified

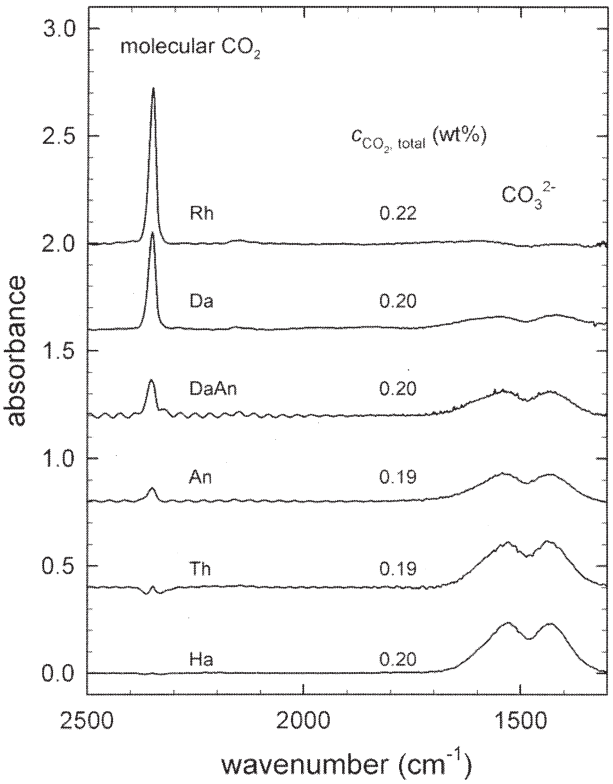

Fig. 2. Volatile-free background corrected mid-infrared spectra of CO_2-bearing Rh to Ha glasses normalized to 100 μm thickness. Total CO_2 concentrations have been determined by weight considering the measured CO_2 yield of silver oxalate.

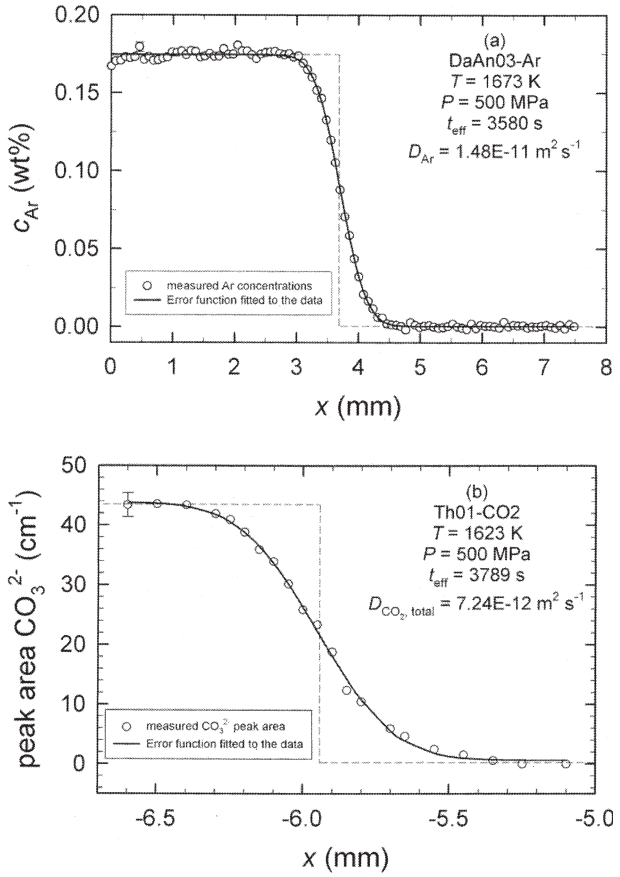

Fig. 3. (a) Typical Ar concentration distance profile. Error in c_{Ar} is about the size of symbols. (b) Typical CO_3^{2-} peak area distance profile. The given error bar in peak area is representative for all data points. The dashed lines in (a) and (b) represent the steps in concentration at the beginning of the experiments.

error function to the measured Ar concentrations and estimated CO_2 concentration distance profiles (Crank, 1975):

$$c_{x,t} = c_{min} + \frac{(c_{max} - c_{min})}{2} [1 - erf((x - x_M)d)] \quad (2)$$

In Eqn. 2, c is the concentration at time t at position x, c_{min} is the minimum volatile concentration, c_{max} is the maximum volatile concentration, and x_M is the position of the Matano-interface. The diffusion coefficient D can be calculated from parameter d:

$$D = \frac{1}{4(d)^2 t} \quad (3)$$

where t (in s) is the duration of the experiment.

3.3. Sources of Error

In diffusion experiments on low viscosity melts convection of melt may contribute to the transport of diffusing species. Convection processes require density gradients induced by (1) temperature gradients and/or (2) differences in melt composition. In contrast to piston cylinder experiments the temperature gradients in our experiments performed in an IHPV are very small (~2 to 3 K over the length of a diffusion sample). Differences in density of our volatile-bearing and volatile-free samples are negligible because of low Ar and CO_2 concentrations (Table 1). Furthermore, melt convection processes would distort the shapes of the concentration distance profiles producing curves that are inconsistent with the forms of error functions. Neither the concentration distance profiles nor the internal consistency of the Ar diffusion data suggest melt convection processes in our experiments.

Nevertheless we checked for possible melt convection in low viscous melts that may contribute to volatile transport and that may deform the Matano interface. We analysed the Ar gradation of the sample Ha04-Ar with the lowest viscosity. In a first step 7 Ar concentration distance profiles were monitored parallel to each other with an offset of 350 μm (Fig. 4a). Analysis of the profiles give an $\log D_{Ar}$ (in $m^2\ s^{-1}$) of -9.92 with a standard error of the mean of ± 0.05 log unit. In a second step 5 Ar concentration profiles perpendicular to the direction of diffusion were analysed in the Ar-free part, near the Matano interface, and in the Ar-rich part of the sample (Fig. 4b). Within error these Ar concentration profiles show a constant Ar gradation indicating that melt convection did not disturb our diffusion experiments.

In most Ar diffusion experiments, the melts quenched to glasses free of crystals. The diffusion samples Rh01-Ar and Da01-Ar run at 1373 K and 1473 K, respectively, contain few crystals indicating that near-liquidus temperatures were reached. The phase proportions of the crystals were determined by using back-scattered electron images in combination with ImageAnalysis 3.0 software. The amount of these crystals 1 to 2 μm across and up to 25 μm long is less than 1 vol%. The very low proportion of the crystals and the internal consistency of our Ar diffusion data suggest that the presence of these crystals appears to have no effect on the determination of Ar diffusivity within error.

Furthermore, all Ar diffusion samples contain small amounts of homogeneously distributed H_2O tested by several IR measurements at the rims and in the middle of the samples. This might have some slight effect on the Ar diffusion rate. The mid-infrared spectra of four Ar diffusion samples showing the fundamental OH-stretching band are presented in Figure 5. We used the peak height, the extinction coefficient of 67 L mol^{-1} cm^{-1} given by Stolper (1982), and the density calculation for the glass compositions of Appen (1949, 1957) to calculate the total H_2O contents. The total H_2O contents range from 0.27 $\pm$ 0.04 wt% in the rhyolitic diffusion sample to 0.05 $\pm$ 0.02 wt% in the dacitic samples (Table 1). The total H_2O contents in the Ar/CO_2-free and Ar/CO_2-bearing parts of the individual diffusion samples deviate only 0.04 wt% in Ar diffusion experiments with Rh composition to 0.02 wt% in all other diffusion pairs thus having negligible influence on Ar and total CO_2 mobility in the diffusion samples.

A number of additional sources of error may affect the determination of Ar and total CO_2 diffusivity in the experiments. The major uncertainties in diffusion coefficients are uncertainties in temperature, diffusion time, distance, and concentration of Ar or peak area of CO_2 and/or CO_3^{2-}. The uncertainty in T is estimated to be ± 10 K. The effective diffusion time t_{eff} is larger than the nominal time t_{nom} at

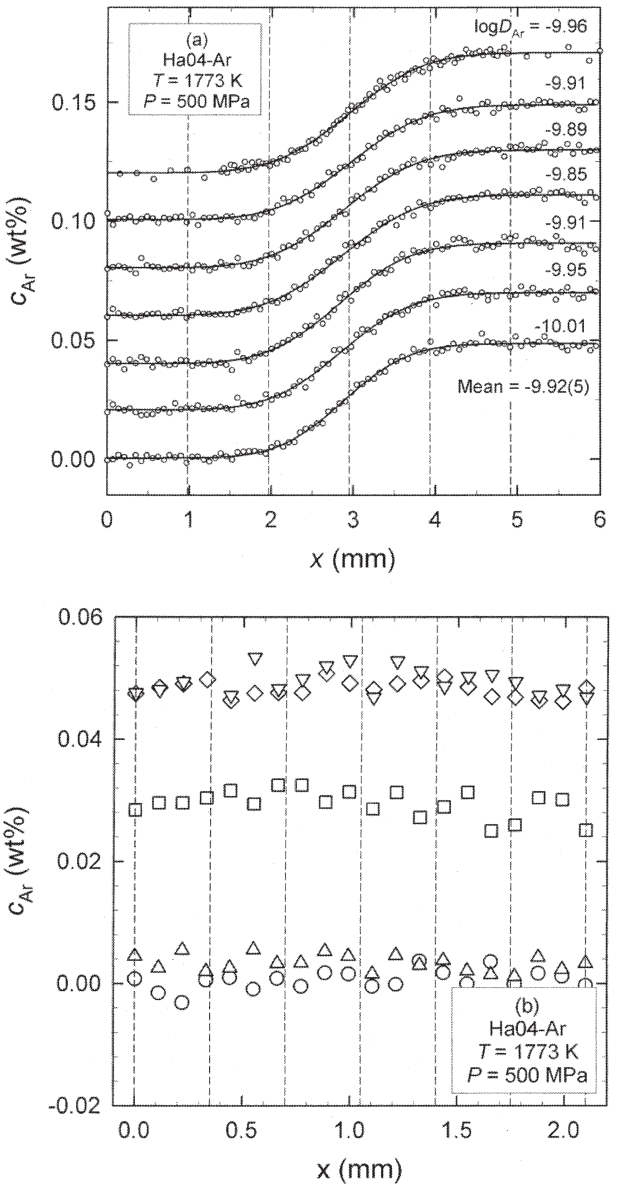

Fig. 4. (a) Ar concentration distance profiles of diffusion sample Ha04-Ar measured with an offset of n × 350 μm (n = 1–7) parallel to the diffusion direction of Ar. Profiles are shifted for clarity. Solid lines represent best fit error functions and dashed lines represent positions of Ar concentration distance profiles measured perpendicular to the diffusion direction of Ar shown in (b). Dashed lines in (b) represent positions of profiles shown in (a).

which the samples are hold at run conditions because diffusion of volatiles already takes place during heating to run temperature and continues during cooling after the experiments. The effective run time was obtained by correcting the nominal diffusion time for the time required for heating and cooling by an iterative procedure described by Nowak and Behrens (1997). For the isothermal CO_2 diffusion experiments we used an activation energy of total CO_2 diffusion of 195 kJ/mol (Watson, 1994) to calculate effective run times. The error in t_{eff} is estimated to be 60 s, 0.15 to 3% of the effective run time. An additional source of error is the determination of the position x in the distance of the diffusion profiles. The error in measurement of the position is estimated to be 1 μm in the Ar profiles and thus negligible and 10 μm in the CO_2 peak area profiles. The error in profile length is defined by the angle deviation α from the diffusion direction of the volatiles. The deviation of the diffusion coefficient D in % can be obtained from $(1 - \cos^{2\alpha}) \times 100$. Deviation of the measured profile from the diffusion direction is estimated to be less than 10° resulting in a maximum overestimation of the D values of 3% relative.

Furthermore, the fitting parameter d in Eqn. 3 from which diffusion coefficients are extracted, is a source of error that includes the uncertainty in concentration (4% rel. for Ar and 10% rel. for the sum of peak areas of molecular CO_2 and CO_3^{2-}). The uncertainty in the pressure calibration at 500 MPa is ±5 MPa and has no significant influence on the diffusion data because of the relatively small pressure dependence of Ar (Carroll, 1991; Roselieb et al., 1996; Behrens and Zhang, 2001) and total CO_2 (Watson, 1994).

Eqn. 4 combines the discussed individual errors to calculate the relative error in diffusivity.

$$\frac{\Delta D}{D} = \sqrt{\left[\left(\left(\frac{-E_A}{R}\right)\cdot\left(-\frac{1}{T^2}\right)\cdot\Delta T\right)^2 + \left(\frac{\Delta t_{eff}}{t_{eff}}\right)^2 + \left(\frac{2\Delta x}{x}\right)^2 ?+ \left(\frac{2\Delta d}{d}\right)^2\right]} \quad (4)$$

Error analysis results in errors of about ±0.05 log units for Ar diffusivities and about ±0.1 log units for total CO_2 diffusivities. However, experimental reproducibility of a diffusion couple experiment is not quite as good as an error analysis on one experiment indicates it should be. The scatter in the Arrhenius diagram (Fig. 6a) suggests uncertainties in D_{Ar} about ±0.1 log unit and Sierralta (2002) suggests uncertainties in $D_{CO_{2,total}}$ ~0.15 log unit.

To check for reproducibility and time independence of diffusion two CO_2 diffusion runs and two Ar diffusion runs with different run times were performed with DaAn composition (DaAn01-CO2: t_{nom} = 3600 s, DaAn02-CO2: t_{nom} = 14,520 s) and with Rh composition (Rh04-Ar: t_{nom} = 3420 s, Rh05-Ar:

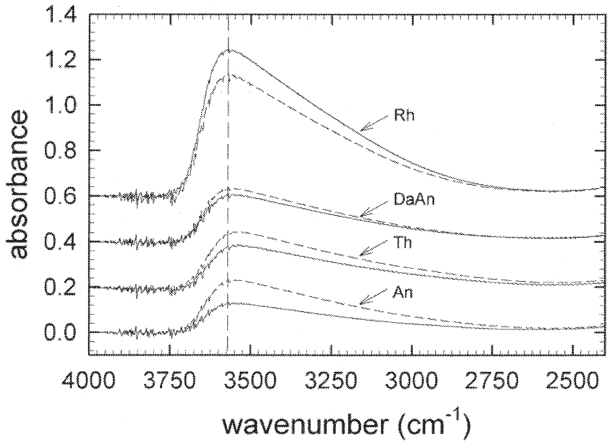

Fig. 5. Mid-infrared spectra of Ar-free (solid lines) and Ar-bearing (dashed lines) glass samples normalized to 250 μm thickness. The absorption bands with the maximum at ~3620 cm^{-1} are due to the fundamental OH stretching vibration. Spectra are shifted for clarity.

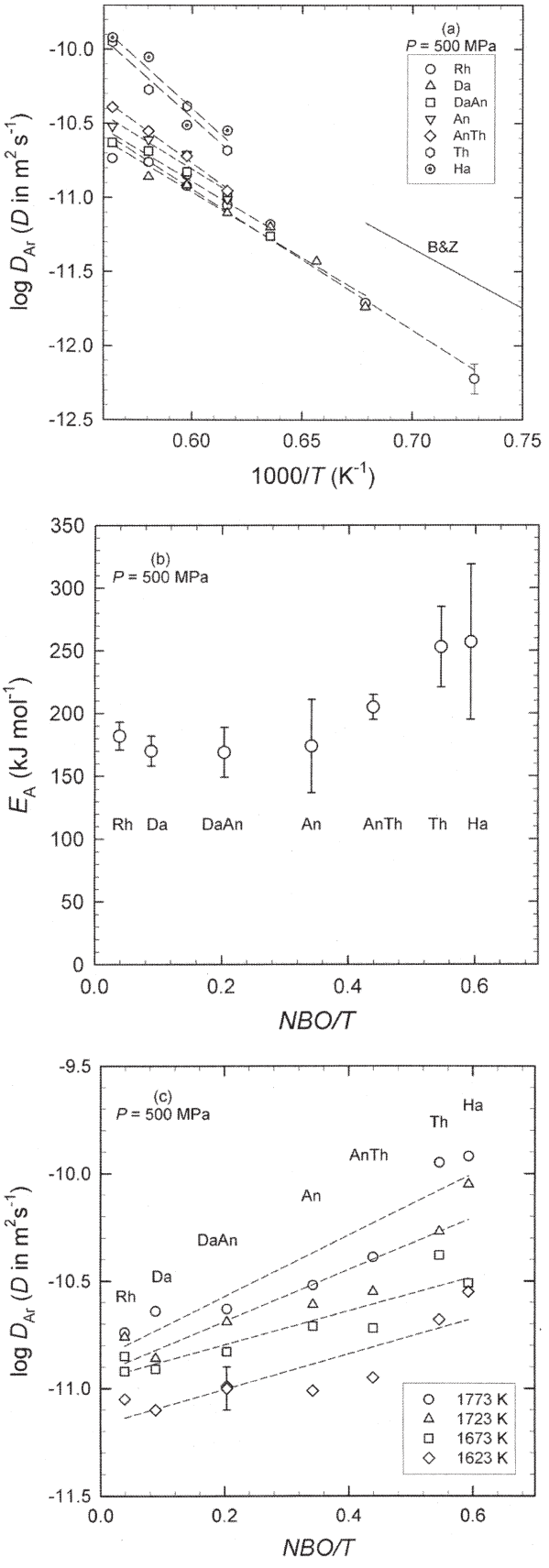

Fig. 6. (a) Temperature dependence of Ar diffusivity in Rh to Ha melts. The given error bar is representative for all data points. B&Z: Ar diffusivity for rhyolitic melt with 0.27 wt% H_2O at 500 MPa calculated from Behrens and Zhang (2001). Dashed lines represent best linear fits. (b) Activation energy for Ar diffusion vs. *NBO/T*. Error bars result from error propagation calculations. (c) Diffusivity of Ar vs. *NBO/T* for temperatures ranging from 1623 to 1773 K. The given error bar is representative for all data points. Dashed lines represent best linear fits.

t_{nom} = 2460 s). Both determined CO_2 diffusion coefficients are identical within error ($\log D_{CO_{2,total}} = -11.14$ for DaAn01 and -11.18 for DaAn02; $\log D_{Ar} = -10.92$ for Rh04-Ar and -10.85 for Rh05-Ar; D in m^2 s^{-1}) demonstrating that D is independent of time implying that the CO_2 transport process is controlled by diffusion.

3.4. Diffusion Data of Ar in Silicate Melts

In the investigated temperature range the mobility of Ar increases exponentially with increasing temperature. The data are summarized in Table 2 and in Figure 6a. In addition to the diffusion rates of Rh to AnTh, the diffusion data for Th and Ha melts were also used to constrain the activation energies, although showing significant scatter and the smallest temperature range. Linear regression lines were fitted to each composition. The slope of the best fit lines provide the activation energy E_A for Ar diffusion and the y-axis intercept at $x = 0$ provides the preexponential factor of Eqn. 5:

$$D_{Ar} = D_0 \cdot e^{\left(\frac{-E_A}{RT}\right)} \quad (5)$$

The fit parameters, and derived activation energies shown in Figure 6b together with fit standard errors are given in Table 3. Figure 6c shows that Argon diffusion at 1623 to 1773 K increases exponentially with the degree of depolymerisation expressed as the ratio of non bridging oxygen atoms per tetrahedral cations (*NBO/T*) calculated from Mysen (1988).

3.5. Diffusion Data of CO_2 in Rh to Ha

The results of the isothermal CO_2 diffusion experiments at 1623 K and 500 MPa are summarized in Table 2 and Figure 7. Within error, the diffusion data show clearly that in contrast to Ar diffusion, the CO_2 diffusion is independent of bulk composition in the simplified natural melts studied. Furthermore, within error at 1623 K the diffusivity of Ar is identical to the total CO_2 diffusivity in Rh melt, consistent to the data of Behrens and Zhang (2001).

4. DISCUSSION

4.1. Ar Diffusion and Activation Energy

The activation energies E_A of Ar diffusion at 500 MPa range from 169 ± 20 kJ mol^{-1} at 1573 to 1773 K in DaAn melt to ~257 ± 62 kJ mol^{-1} at 1623 K to 1773 K in Ha melt (Table 3 and Fig. 6b). A dependence of E_A on bulk composition is difficult to show because of the large errors in E_A. For Rh melt we determined an E_A of 182 ± 11 kJ mol^{-1} for a pressure of 500 MPa and temperatures ranging from 1373 to 1773 K. For

a similar melt composition Carroll (1991) determined an E_A of 144 ± 6 kJ mol^{-1} at pressures and temperatures ranging from 128 to 373 MPa and 773 to 1173 K. Using Behrens and Zang (2001) we calculated for rhyolitic melt an E_A of 156 ± 4 kJ mol^{-1} at a pressure of 500 MPa, temperatures ranging from 753 K to 1373 K, and a total H_2O content of 0.27 wt%. Using Behrens and Zhang (2001) the calculated Ar diffusivities for rhyolitic melt are half a log unit higher compared to our measurements. The observed difference in absolute Ar diffusivity and in E_A might be related to a significantly higher MgO and CaO concentration in our Rh composition.

4.2. CO_2 Diffusion

Recently, Sierralta et al. (2002) have suggested that in the system $NaAlSi_3O_8$ + nNa_2O (n = 0–6.9 wt%) at 1523 K and 500 MPa the diffusivity of bulk CO_2 increases exponentially with Na_2O and H_2O content and thus exponentially with *NBO/T*. The bulk CO_2 diffusivity increases from $\log D_{CO_{2,total}}$ = −11.38 (D in m^{2}s^{-1}) in $NaAlSi_3O_8$ melt with *NBO/T* close to zero to $\log D_{CO_{2,total}}$ = −10.92 in $NaAlSi_3O_8$ melt containing 6.9 wt% Na_2O excess with *NBO/T* of 0.156. In contrast, the bulk CO_2 diffusion data of this study appear to be insensitive to changes over a range of more complex melt compositions from Rh with *NBO/T* = 0.041 (close to zero) to Ha melt with *NBO/T* = 0.583. This observation is consistent with the diffusion data in simple sodium aluminosilicate melt and haplobasaltic melt of Watson et al. (1982). At first sight, the different behaviour of CO_2 mobility in simple $NaAlSi_3O_8$ + nNa_2O melts and more complex iron free natural melts appears contrary but the CO_2 mobility over the range of compositions studied may reflect a combination of several effects. There are three possible explanations for the different behaviour of CO_2 mobility. Firstly, different behaviour of changes in CO_2 speciation with degree of depolymerisation may affect CO_2 mobility. Secondly, different behaviour of changes in the individual diffusion coefficients of molecular CO_2 and CO_3^{2-} with bulk composition may change CO_2 mobility. Lastly, in depolymerised $NaAlSi_3O_8$ + nNa_2O glasses/melts there appears to be the possibility of a further 'ionic pair' type of carbonate with the ability to move faster than carbonates more intimately associated with the network (Brooker et al., 2001b). These are the very species that become prevalent in peralkaline glasses eventually forming a sublattice that leads to immiscible separation of silicate and carbonate melts. In this case it is the peralkalinity of the melt rather than the *NBO/T* that might control the abundance of these species and the resulting diffusion rate.

However, neither individual diffusivities of CO_2 species nor the CO_2 species concentrations in the melt can be extracted directly from the CO_2 diffusion experiments. During diffusional processes in the melt, the equilibrium between the CO_2 species is locally maintained and the equilibrium concentrations of species are known to be unquenchable to room temperature for some melt compositions (Nowak et al., 2003).

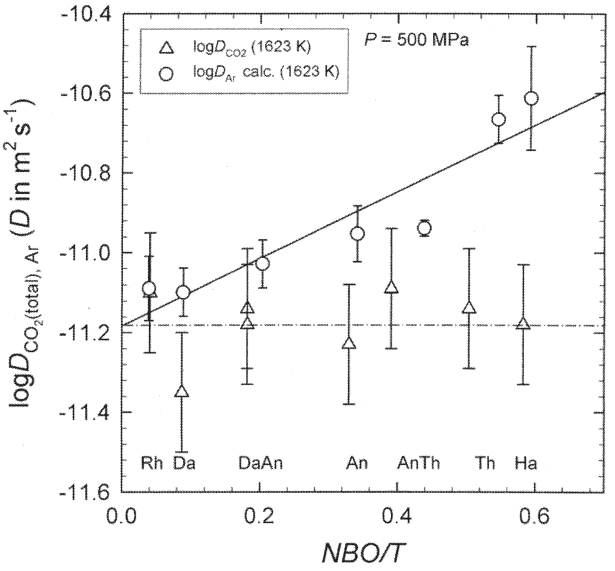

Fig. 7. Diffusivity of Ar and total CO_2 vs. *NBO/T*. The diffusivity of total CO_2 at 1623 K is independent of bulk melt composition. The averaged value $\log D_{CO_{2,total}}$ is −11.18 ± 0.08 represented by the dashed dotted line. Argon diffusivity can be described by $\log D_{Ar}$ = −11.18(6) + 0.79(15) *NBO/T* represented by the straight line (r^2 = 0.79, fit standard error = 0.08).

4.3. Comparison of Ar Diffusion with Total CO_2 Diffusion

In contrast to the diffusion of the reactive component CO_2 the diffusion of the inert component Ar increases exponentially with *NBO/T*. Figure 7 shows the measured diffusion data at 1623 K of total CO_2 and the diffusion data of Ar calculated from the Arrhenius equations for the whole range of compositions studied based on 7 data points for Rh, 7 data points for Da, 5 data points for DaAn, and 4 data points for An, AnTh, Th, and Ha composition (Table 2, Table 3, and Fig. 6a). The Ar diffusion data at 1623 K can be expressed as

$$\log D_{Ar} = -11.18(6) + 0.84(15) NBO/T \quad (6)$$

Table 3. Linear regression parameters of $\log D_{Ar}$ vs. 1000/T (K) values and extracted activation energies for Ar diffusion ($\log D_{Ar} = a + b1000/T$)

	a	b	r^2	Fit standard error	E_A (kJ mol^{-1})
Rh	−5.23 (36)	−9.51 (57)	0.97	0.08	182 (11)
Da	−5.64 (38)	−8.86 (61)	0.98	0.06	170 (12)
DaAn	−5.60 (63)	−8.81 (1.05)	0.96	0.06	169 (20)
An	−5.34 (1.13)	−9.11 (1.91)	0.92	0.07	174 (37)
AnTh	−4.34 (31)	−10.71 (52)	0.99	0.02	205 (10)
Th	−2.52 (99)	−13.22 (1.67)	0.97	0.06	253 (32)
Ha	−2.35 (1.92)	−13.41 (3.26)	0.89	0.13	257 (62)

with an r^2 value of 0.79 and a fit standard error of 0.08. Increasing mobility of the inert component Ar with *NBO/T* supports the idea of Behrens and Nowak (1997) and Zhang and Behrens (2000) that the diffusivity of molecular species like molecular H_2O in rhyolitic melts increases with total H_2O content and thus with increasing *NBO/T*.

4.4. Development of CO_2 Diffusion Model

A mathematical description of diffusion in one dimension is given by Fick's first law

$$J_i = -D_i \frac{\partial c_i}{\partial x} \tag{7}$$

where J_i is the flux, D_i is the diffusion coefficient, c_i is the concentration of the diffusing species *i,* and x is the distance in direction of diffusion. Assuming CO_2 is dissolved and diffuses in two forms, molecular CO_2 and CO_3^{2-}, the total flux of CO_2 is given by:

$$J_{CO_2,\ total} = J_{CO_2,\ molecular} + J_{CO_3^{2-}} \tag{8}$$

If Eqn. 7 is combined with Eqn. 8, a simple rearrangement gives the diffusion of total CO_2:

$$D_{CO_2,\ total} = D_{CO_2,\ molecular} \frac{\partial c_{CO_2,\ molecular}}{\partial c_{CO_2,\ total}} + D_{CO_3^{2-}} \frac{\partial c_{CO_3^{2-}}}{\partial c_{CO_2,\ total}} \tag{9}$$

This approach is similar to the treatment of one-dimensional diffusion of the reactive component H_2O in silicate glasses and melts (Doremus, 1969; Tomozawa, 1985; Wasserburg, 1988; Checkhmir et al., 1989; Zhang et al., 1991). Assuming, that during diffusional processes in the melt, the equilibrium between the CO_2 species (molecular CO_2 and CO_3^{2-}) is locally maintained and that the mole fraction of molecular CO_2 ($nCO_{2,\ molecular}/(nCO_{2,\ molecular} + nCO_3^{2-})$) is independent of total carbon concentration for the same bulk composition (Fine and Stolper, 1985) we can write:

$$\frac{\partial c_{CO_2,molecular}}{\partial c_{CO_2,\ total}} = x_{CO_2,\ molecular} \tag{10}$$

where $x_{CO_2,\ molecular}$ is the mole fraction of molecular CO_2 and

$$\frac{\partial c_{CO_3^{2-}}}{\partial c_{CO_2,\ total}} = x_{CO_3^{2-}} \tag{11}$$

where $x_{CO_3^{2-}}$ is the mole fraction of CO_3^{2-}.

Substituting Eqn. 10 and 11 into Eqn. 9 gives:

$$D_{CO_2,\ total} = D_{CO_2,\ molecular}\ x_{CO_2,\ molecular} + D_{CO_3^{2-}} x_{CO_3^{2-}} \tag{12}$$

The sum of the constants $x_{CO_2,\ molecular}$ and $x_{CO_3^{2-}}$ has to be:

$$x_{CO_2,\ molecular} + x_{CO_3^{2-}} = 1 \tag{13}$$

Substituting $x_{CO_3^{2-}}$ in Eqn. 12 we have:

$$D_{CO_2,\ total} = D_{CO_2,\ molecular}\, x_{CO_2,\ molecular} + D_{CO_3^{2-}}(1 - x_{CO_2,\ molecular}) \tag{14}$$

After rearrangement of Eqn. 14 we find:

$$D_{CO_3^{2-}} = \frac{D_{CO_2,\ total} - D_{CO_2,\ molecular}\, x_{CO_2,\ molecular}}{(1 - x_{CO_2,\ molecular})} \tag{15}$$

or alternatively:

$$x_{CO_2,\ molecular} = \frac{D_{CO_2,\ total} - D_{CO_3^{2-}}}{D_{CO_2,\ molecular} - D_{CO_3^{2-}}} \tag{16}$$

4.5. Application of the Diffusion Model for Da Composition

In principle, Eqn. 15 allows the calculation of $D_{CO_3^{2-}}$ if total CO_2 diffusion, molecular CO_2 diffusion, and the mole fraction $x_{CO_2,\ molecular}$ are known which is the case for Da composition. The total CO_2 diffusion is determined experimentally. The averaged total CO_2 diffusion in Rh to Ha melts at 1623 K and 500 MPa is $6.61 \times 10^{-12} \pm 1.22 \times 10^{-12}$ m^2 s^{-1}. Behrens and Zhang (2001) have recently demonstrated that in rhyolitic melt, that dissolve CO_2 almost entirely as molecular species, the diffusion rate of the spherical molecule Ar with a radius of 1.64 Å (Zhang, 1995) is almost identical to the diffusion rate of the cylindrical shaped CO_2 molecules with a base radius of 1.4 Å and a length of ~5 Å (Wood and Nassau, 1967). This diffusion behaviour has been confirmed by our results (Table 4). Behrens and Zhang (2001) suggest that the smaller base radius compensates for the greater length of the CO_2 molecule compared to the size of the Ar atom and that the linear CO_2 molecule moves parallel to its cylindrical axis to minimize expansion of the doorways of the silicate network similar to diffusion of molecular CO_2 in channels of cordierite heated at 1073 K (Aines and Rossman, 1984). If we speculate that the diffusion rate of molecular CO_2 might be the same as Ar in the silicate melt compositions Rh to Ha, then we can use D_{Ar} (1673 K: $7.94 \times 10^{-12} \pm 1.83 \times 10^{-12}$ m^2 s^{-1}) as a proxy for $D_{CO_2,\ molecular}$ in Da melt.

We also need to estimate the proportion of molecular CO_2 species present in the melt at the conditions of the diffusion experiment as opposed to the ratio observed in the quenched glass. Recently, the CO_2 speciation in albitic and dacitic glasses has been estimated at the glass transition temperature using infrared spectroscopy (Nowak et al., 2003). The annealing temperature dependent CO_2 species concentrations and an ideal solution model were used to determine equilibrium constants for the homogeneous CO_2 species reaction. We derived values for the enthalpy $\Delta H°$ and entropy $\Delta S°$ of this reaction in dacite ($\Delta H° = -29 \pm 2$ kJ mol^{-1} and $\Delta S° = -32 \pm 3$ J mol^{-1} K^{-1}). The equilibrium constant K for the CO_2 species reaction is defined as:

$$\ln K = \frac{-\Delta H}{RT} + \frac{\Delta S}{R} \tag{17}$$

Extrapolating the experimentally determined thermodynamic parameters from temperatures nearby the glass transition temperature to the temperature of the CO_2 diffusion run at 1623 K we obtain $K = 0.183 \pm 0.095$.

Table 4. Compilation of molecular CO_2, CO_3^{2-} and Ar diffusion data, CO_2 speciation data expressed as $x_{CO_2,\ molecular}$, and contribution of molecular CO_2 diffusion on total CO_2 diffusion at 1623 K and 500 MPa. All log$D$ data are given in $m^2\ s^{-1}$

	Rh	Da	DaAn	An	AnTh	Th	Ha
$\log D_{CO_2,total}$ [a]	−11.18 (8)	−11.18 (8)	−11.18 (8)	−11.18 (8)	−11.18 (8)	−11.18 (8)	−11.18 (8)
$\log\eta$ (η in Pas)[b]	4.80 (48)	3.81 (38)	2.80 (28)	2.18 (22)	1.87 (19)	1.61 (16)	1.50 (15)
$\log D_{CO_3^{2-}}$ [b]	−14.93 (48)	−13.94 (38)	−12.93 (28)	−12.30 (21)	−12.00 (19)	−11.73 (16)	−11.63 (15)
$\log D_{Ar}$ (Arrh.)[c]	−11.09 (8)	−11.10 (6)	−11.03 (6)	−10.95 (7)	−10.94 (2)	−10.67 (6)	−10.61 (13)
$\log D_{Ar}$ (*NBO/T*)[d]	−11.15 (8)	−11.11 (8)	−11.01 (8)	−10.89 (8)	−10.81 (8)	−10.72 (8)	−10.68 (8)
$x_{CO_2,\ molecular}$ (Arrh.)[e]	0.81 (21)	0.83 (19)	0.70 (17)	0.57 (15)	0.53 (12)	0.24 (8)	0.19 (9)
$x_{CO_2,\ molecular}$ (mod.)[f]	0.93 (24)	0.85 (22)	0.67 (18)	0.49 (14)	0.39 (12)	0.28 (10)	0.23 (9)
$\Delta x_{CO_2,\ molecular}$ (absolute)	0.12	0.02	−0.03	−0.08	−0.14	0.04	0.04
$\Delta x_{CO_2,\ molecular}$ (%)	12.9	2.3	−4.8	−15.5	−38.2	11.9	16.8
Contribution of $D_{CO_2,\ molecular}$ to $D_{CO_2,\ total}$	1.00	1.00	0.99	0.96	0.91	0.80	0.73

[a] Averaged total CO_2 diffusion at 1623 K.
[b] Calculated from viscosity model of Giordano and Dingwell (2003) and the Eyring equation using a jump distance of 3×10^{-10} m.
[c] $\log D_{Ar}$ (Arrhenius) = data calculated from linear regressions of Arrhenian plots (Fig. 6a, Table 3).
[d] $\log D_{Ar}$ (*NBO/T*) = calculated from Eqn. 6.
[e] $x_{CO_2,\ molecular}$ (Arrhenius) is based on a, b, and c.
[f] $x_{CO_2,\ molecular}$ (modelled) is based on a, b, and d.

Combining the following equations

$$K = \frac{[CO_3^{2-}]}{[CO_{2,\ molecular}] \cdot [O^{2-}]} \tag{18}$$

where $[CO_3^{2-}]$, $[CO_{2,\ molecular}]$, and $[O^{2-}]$ are the molar fractions of CO_3^{2-}, CO_2 molecules, and oxygen of the melt, respectively, with

$$[CO_3^{2-}] + [CO_{2,\ molecular}] + [O^{2-}] = 1 \tag{19}$$

and

$$[CO_{2,\ total}] = [CO_3^{2-}] + [CO_{2,\ molecular}] \tag{20}$$

we end up with the following equation:

$$[CO_{2,\ molecular}] = \frac{[CO_{2,\ total}]}{K(1 - [CO_{2,\ total}]) + 1} \tag{21}$$

Using this equation we obtain a value of 0.86 ± 0.06 for $[CO_{2,\ molecular}]$ which is identical to $x_{CO_2,\ molecular}$. In this case the diffusion coefficient of CO_3^{2-} is $-1.56 \times 10^{-12} \pm 1.48 \times 10^{-11}$ $m^2\ s^{-1}$. This result shows that the uncertainty of individual diffusion coefficients for total CO_2 and Ar diffusion and of the calculated ratio $x_{CO_2,\ molecular}$ is too high to extract a precise value for the mobility of CO_3^{2-}.

According to generally accepted models, CO_3^{2-} groups with the IR doublet signature observed for the compositions of this study (see Fig. 2) are bonded to the silicate network in some way (Stolper et al., 1987; Kohn et al., 1991; Brooker et al., 1999, 2001a,b). Baker (1990) investigated the interdiffusion of dry dacite and rhyolite. Diffusion coefficients of the network formers Si and Al at 1623 K are on the order of 10^{-13} to 10^{-14} $m^2\ s^{-1}$, 2–3 orders of magnitude slower than diffusion of Ar or molecular CO_2. If the mobility of bulk CO_2 in silicate melts requires the interconversion of CO_3^{2-} into molecular CO_2, a jump into an adjacent site and back reaction to CO_3^{2-} (e. g. Kubicki and Stolper, 1995) and we assume that the mobility of CO_3^{2-} fixed to the silicate network is comparable to the much slower diffusion rate of the network forming cations, then the flux of CO_3^{2-} in dacitic melt can be neglected. Following this argument, Eqn. 12 can be simplified and in first approximation the diffusivity of total CO_2 is given by:

$$D_{CO_2,\ total} = D_{CO_2,\ molecular} x_{CO_2,\ molecular} \tag{22}$$

This equation can be used to calculate the fraction of molecular CO_2 with the diffusion coefficient of total CO_2 and molecular CO_2. This calculation gives 0.83 ± 0.24 for $x_{CO_2,\ molecular}$ which is only 4% lower than the fraction of molecular CO_2 extrapolated to 1623 K from annealing experiments (Nowak et al., 2003).

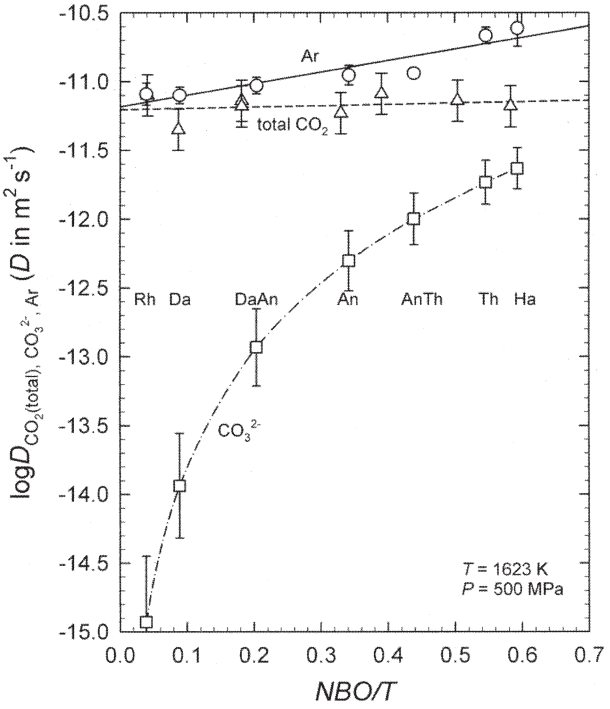

Fig. 8. Diffusivities of total CO_2, Ar and the diffusivity of network former components as a proxy for diffusivity of CO_3^{2-} vs. *NBO/T*.

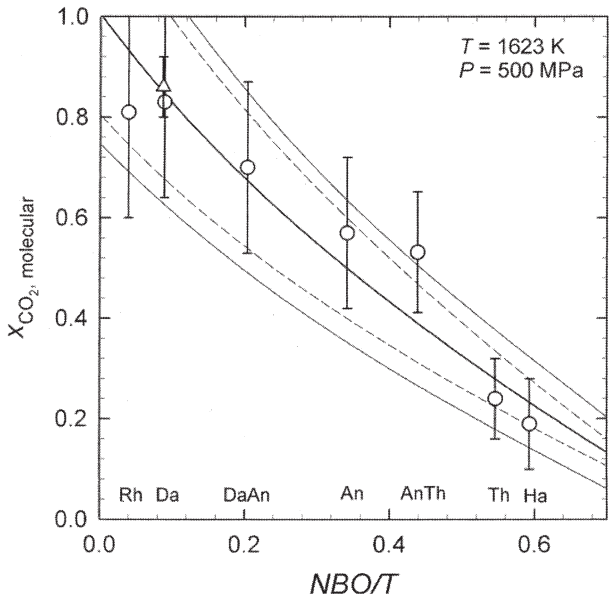

Fig. 9. The $x_{CO_2,\ molecular}$ vs. *NBO/T* at 1623 K and 500 MPa. The thick line is calculated using Eqn. 16, input data are Ar diffusion calculated from Eqn. 6, averaged total CO_2 diffusion, and CO_3^{2-} diffusion calculated from viscosity data (Table 4). Thin solid lines represent the error of the model. Dashed lines represent an error of ±20% of the modeled $x_{CO_2,\ molecular}$ values. Circles are calculated from Ar diffusion data obtained from linear regressions of Arrhenian plots (Fig. 6a and Table 3), averaged total CO_2 diffusion and CO_3^{2-} diffusion calculated from viscosity data. The triangle represents the CO_2 speciation extrapolated from the thermodynamic parameters ΔH and ΔS for Da composition (Nowak et al., 2003).

For more depolymerised melts the contribution of CO_3^{2-} to total CO_2 diffusion may become far more significant. In the next section we attempt to model CO_2 speciation in the melt using the assumption that the CO_3^{2-} diffusion rate is identical to that of the network formers, and Ar diffusion is used as a proxy for molecular CO_2 diffusion in the whole range of melt compositions studied.

4.6. Application of the Diffusion Model to Other Melt Compositions

Recently, Giordano and Dingwell (2003, 2004) published a non-Arrhenian multicomponent viscosity model for silicate melts. The model reproduces melt viscosities to within <10% on a logarithmic scale. The viscosity model correlated to *NBO/T* (Giordano and Dingwell, 2004):

$$\log_{10}\eta = a_1 \cdot \ln(NBO/T - a_2) + a_3 \quad (23)$$

(1623 K: $a_1 = -1.22177$, $a_2 = -0.00098$, $a_3 = 0.86842$) can be used in combination with the Eyring equation:

$$D_{CO_3^{2-}} = \frac{k \cdot T}{\lambda \cdot \eta} \quad (24)$$

(k Boltzmann constant, T temperature in K, λ jump distance, η viscosity in Pas) to calculate the mobility of CO_3^{2-} assuming that this component is linked to the melt network structure. We used a jump distance of 3×10^{-10} m for network former diffusion. This value was recently confirmed by Koepke and Behrens (2001) for the chemical diffusivity of high field strength elements (HFSE) like Zr^{4+} in both, dry and hydrous melts that is similar to Si^{4+} and Al^{3+} diffusion. The diffusivity of network former components as a proxy for CO_3^{2-} mobility together with total CO_2 diffusion and Ar diffusion is given in Figure 8. Figure 9 shows $x_{CO_2,\ molecular}$ calculated with Eqn. 16 vs. *NBO/T* at 1623 K and 500 MPa together with data points using total CO_2, calculated network former diffusion rate as a proxy for CO_3^{2-} mobility, and calculated Ar diffusivity from the Arrhenian fits (Table 3) as a proxy for molecular CO_2 mobility for the individual melt compositions. Input data and errors are compiled in Table 4.

Six of seven data points match the model within 20%. The model demonstrates that (1) $x_{CO_2,\ molecular}$ decreases with *NBO/T* and (2) even in the highly depolymerised melt compositions (e.g., Ha and Th; Table 4) molecular CO_2 is a stable species and contributes 70 to 80% to total CO_2 diffusion, respectively.

The determination of CO_2 speciation using diffusion data are a promising approach and an alternative to high pressure high temperature in situ spectroscopic studies that are difficult to perform in depolymerised melt systems. Further Ar diffusion studies will be performed to shed light on total CO_2 diffusion and CO_2 speciation in the system $NaAlSi_3O_8$ + nNa_2O and to test the CO_2 diffusion/speciation model.

Acknowledgments—This study is supported by the Deutsche Forschungsgemeinschaft (SPP NO 378/2). The authors would like to thank Bruce Watson, Richard Brooker, and an anonymous reviewer for their constructive comments.

Associate editor: J. K. Russell

REFERENCES

Aines R. D. and Rossman G. R. (1984) The high temperature behavior of water and carbon dioxide in cordierite and beryl. *Am. Mineral.* **69,** 319–327.

Appen A. A. (1949) Berechnung der optischen Eigenschaften, der Dichte und des Ausdehnungskoeffizienten von Silikatgläsern aus ihrer Zusammensetzung. *Ber. Akad. Wiss. UdSSR* **69,** 841–844.

Appen A. A. (1957) Some "anomalies" in the properties of glass. In *Travaux du IVe congrès international du verre,* pp. 36–40. Paris.

Baker D. R. (1990) Chem. interdiffusion of dacite and rhyolite: Anhydrous measurements at 1 atm and 10 kbar, application of transition state theory and diffusion in zoned magma chambers. *Contrib. Mineral. Petrol.* **104,** 407–423.

Behrens H. and Nowak M. (1997) The mechanisms of water diffusion in polymerised silicate melts. *Contrib. Mineral. Petrol.* **126,** 377–385.

Behrens H. and Zhang Y. (2001) Ar diffusion in hydrous silicic melts: Implications for volatile diffusion mechanisms and fractions. *Earth Planet. Sci. Lett.* **192,** 363–376.

Berndt J., Liebske C., Holtz F., Freise M., Nowak M., Ziegenbein D., Hurckuck W., and Koepke J. (2002) A combined rapid-quench and H_2-membrane setup for internally heated pressure vessels: Description and application for water solubility in basaltic melts. *Am. Mineral.* **87,** 1710–1716.

Blank J. G. and Brooker R. A. (1994) Experimental studies of carbon dioxide in silicate melts: Solubility, speciation and stable carbon isotope behavior. *Rev. Mineral.* **30,** 157–186.

Brey G., and Green D. H. (1975) The role of CO_2 in the genesis of olivine melilitite. *Contrib. Mineral. Petrol.* **49,** 93–103.

Brooker R. A., Kohn S. C. Holloway J. R., McMillan P. F., and Carroll M. R. (1999) Solubility, speciation and dissolution mechanisms for

CO_2 in melts on the $NaAlO_2$-SiO_2 join. *Geochim. Cosmochim. Acta* **63,** 3549–3565.

Brooker R. A., Kohn S. C., Holloway J. R., McMillan P. F., and Carroll M. R. (2001a) Structural controls on the solubility of CO_2 in silicate melts part I: Bulk solubility data. *Chem. Geol.* **174,** 225–239.

Brooker R. A., Kohn S. C., Holloway J. R., and McMillan P. F. (2001b) Structural controls on the solubility of CO_2 in silicate melts part II: IR characteristics of carbonate groups in silicate glasses. *Chem. Geol.* **174,** 241–254.

Carroll M. R. (1991) Diffusion of Ar in rhyolite, orthoclase and albite composition glasses. *Earth Planet. Sci. Lett.* **103,** 156–168.

Carroll M. R. and Stolper E. M. (1991) Argon solubility and diffusion in silica glass: Implications for the solution behavior of molecular gases. *Geochim. Cosmochim. Acta* **55,** 211–225.

Carroll M. R. and Stolper E. M. (1993) Noble gas solubilities in silicate melts and glasses: New experimental results for argon and the relationship between solubility and ionic porosity. *Geochim. Cosmochim. Acta* **57,** 5039–5051.

Checkhmir A. S., Epel'baum M. B., and Simakin A. G. (1989) Water transport in magmas. *Geochem. Int.* **26,** 125–127.

Crank J. (1975) *The Mathematics of Diffusion.* 2nd ed Oxford University Press.

Doremus R. H. (1969) The diffusion of water in fused silica. In *Reactivity of Solids.* Proceedings of the 6th international symposium on the reactivity of solids. (eds. J. W. Mitchell et al.), pp. 667–673. Wiley-Interscience, New York.

Dowty E. (1980) Crystal-chemical factors affecting the mobility of ions in minerals. *Am. Mineral.* **65,** 174–182.

Fine G. and Stolper E. M. (1985) The speciation of carbon dioxide in sodium aluminosilicate glasses. *Contrib. Mineral. Petrol.* **131,** 323–346.

Fogel R. A. and Rutherford M. J. (1990) The solubility of carbon dioxide in rhyolitic melts: A quantitative FTIR study. *Am. Mineral.* **75,** 1311–1326.

Fortier S. M. and Giletti B. J. (1989) An empirical model for predicting diffusion coefficients in silicate minerals. *Science* **245,** 1481–1484.

Giordano D. and Dingwell D. B. (2003) Non-Arrhenian multicomponent melt viscosity: A model. *Earth Planet. Sci Lett.* **208,** 337–349.

Giordano D. and Dingwell D. B. (2004) Erratum to "Non Arrhenian multicomponent melt viscosity: A model," *Earth Planet. Sci. Lett.* **221,** 449.

Holloway J. R. (1976) Fluids in the evolution of granitic magmas: Consequences of finite CO_2 solubility. *Geol. Soc. Am. Bull.* **87,** 1513–1518.

Koepke J. and Behrens H. (2001) Trace element diffusion in andesitic melts: An application of synchrotron X-ray fluorescence analysis. *Geochim. Cosmochim. Acta* **65,** 1481–1498.

Kohn S. C., Brooker R. A., and Dupree R. (1991) ^{13}C MAS NMR: A method for studying CO_2 speciation in glasses. *Geochim. Cosmochim. Acta* **55,** 3879–3884.

Kubicki J. D. and Stolper E. M. (1995) Structural roles of CO_2 and $[CO_3]^{2-}$ in fully polymerized sodium aluminosilicate melts and glasses. *Geochim. Cosmochim. Acta* **59,** 683–698.

Lange R. A. and Carmichael I. S. E. (1987) Densities of Na_2O-K_2O-CaO-MgO-FeO-Fe_2O_3-Al_2O_3-TiO_2-SiO_2 liquids: New measurements and derived partial molar properties. *Geochim. Cosmochim. Acta* **51,** 2931–2946.

Morizet Y., Kohn S. C., and Brooker R. A. (2001) Annealing experiments on CO_2-bearing jadeite glass: An insight into the true temperature dependence of CO_2 speciation in silicate melts. *Min. Mag.* **65,** 701–707.

Mysen B. O. (1988) *Structure and Properties of Silicate Melts.* Elsevier.

Mysen B. O. and Virgo D. (1980) The solubility behaviour of CO_2 in melts on the join $NaAlSi_3O_8$-$CaAl_2Si_2O_8$-CO_2 at high pressure and temperatures: A Raman spectroscopic study. *Am. Mineral.* **65,** 1166–1175.

Nakamoto K., Fujita J., Tanaka S., and Kobayashi M. (1957) Infrared spectra of metallic complexes. IV. Comparison of the infrared spectra of unidentate and bidentate metallic complexes. *J. Chem. Phys.* **79,** 4904–4908.

Nowak M. and Behrens H. (1997) An experimental investigation on diffusion of water in haplogranitic melts. *Contrib. Mineral. Petrol.* **126,** 365–376.

Nowak M., Porbatzki D., Spickenbom K., and Diedrich O. (2003) Carbon dioxide speciation in silicate melts: A restart. *Earth Planet. Sci. Lett.* **207,** 131–139.

Papale P. and Polacci M. (1999) Role of carbon dioxide in the dynamics of magma ascent in explosive eruptions. *Bull. Volcanol.* **60,** 583–594.

Pawley A. R., Holloway J. R., and McMillan P. F. (1992) The effect of oxygen fugacity on the solubility of carbon-oxygen fluids in basaltic melt. *Earth Planet. Sci. Lett.* **110,** 213–225.

Philpotts A. R. (1990) *Principles of Igneous and Metamorphic Petrology.* Prentice-Hall.

Porbatzki D. and Nowak M. (2001) Annealing CO_2-bearing silicate glasses: A key to quantify CO_2 species in silicate melts? *Beih. z. Eur. J. Mineral. No. 1,* **13,** 143.

Roselieb K., Rammensee W., Büttner H., and Rosenhauer M. (1992) Solubility and diffusion of noble gases in vitreous albite. *Chem. Geol.* **96,** 241–266.

Roselieb K., Rammensee W., Büttner H., and Rosenhauer M. (1995) Diffusion of noble gases in melts of the system SiO_2-$NaAlSi_2O_6$. *Chem. Geol.* **120,** 1–13.

Roselieb K., Büttner H., Eicke U., Köhler U., and Rosenhauer M. (1996) Pressure dependence of Ar and Kr diffusion in jadeitic melt. *Chem. Gol.* **128,** 207–216.

Shannon R. D. and Prewitt C. T. (1969) Effective ionic radii in oxides and fluorides. *Acta Cryst.* B25, 925–946.

Shibata T., Takahashi E., and Matsuda J. (1998) Solubility of neon, argon, krypton and xenon in binary and ternary silicate systems: A new view on noble gas solubility. *Geochim. Cosmochim. Acta* **62,** 1241–1253.

Sierralta M. (2002) Die Diffusion von CO_2 in Natriumaluminosilikatschmelzen: Eine experimentelle Untersuchung zum Einfluss der Zusammensetzung auf die Diffusivität von CO_2. PhD thesis. Hannover, Germany.

Sierralta M., Nowak M., and Keppler H. (2002) The influence of bulk composition on the diffusivity of carbon dioxide in Na aluminosilicate melts. *Am. Mineral.* **87,** 1710–1716.

Stolper E. M. (1982) Water in silicate glasses: An infrared spectroscopic study. *Contrib. Mineral. Petrol.* **81,** 1–17.

Stolper E. M., Fine G. J., Johnson T., and Newman S. (1987) The solubility of carbon dioxide in albitic melt. *Am. Mineral.* **72,** 1071–1085.

Tomozawa M. (1985) Concentration dependence of the diffusion coefficient of water in SiO_2 glass. *J. Am. Ceram. Soc.* **68,** C251–C252.

Wasserburg G. J. (1988) Diffusion of water in silicate melts. *J. Geol.* **96,** 363–367.

Watson E. B., Sneeringer M. A., and Ross A. (1982) Diffusion of dissolved carbonate in magmas: Experimental results and applications. *Earth. Planet. Sci. Lett.* **61,** 346–358.

Watson E. B. (1994) Diffusion in volatile bearing magmas. *Rev. Mineral.* **30,** 371–411.

White W. B. (1974) The carbonate minerals. In *Infrared Spectra of Minerals.* (ed. V. C. Farmer), pp. 227–284. Mineralogical Society of London.

Wood D. L. and Nassau K. (1967) Infrared spectra of foreign molecules in beryl. *J. Chem. Phys.* **47,** 2220–2228.

Zhang Y. (1995) Atomic radii of noble gas elements in condensed phases. *Am. Mineral.*, **80,** 670–675.

Zhang Y., Stolper E. M., and Wasserburg G. J. (1991) Diffusion of water in rhyolitic glasses. *Geochim. Cosmochim. Acta* **55,** 441–456.

Zhang Y. and Behrens H. (2000) H_2O diffusion in rhyolitic melts and glasses. *Chem. Geol.* **169,** 243–262.